ROYAL SIGNALS AND RADAR ESTABLISHMENT

Memorandum 4121

TITLE: PERFORMANCE PREDICTIONS FOR BULK CHALCOGENIDE GRATINGS PRODUCED BY THE PHOTODISSOLUTION EFFECT

AUTHOR: C W Slinger

DATE: February 1988

SUMMARY

Gratings produced by the photodoping of chalcogenide glasses are shown to have great promise for use as diffracting elements in the red to far infrared (up to 15μm). In principle, they are simple to fabricate - phase gratings being produced by mask exposure or holographic techniques. The performance of bulk, rectangular phase gratings is investigated using a coupled wave model and a detailed analysis performed in the thin, multiwave and volume diffraction regimes. High efficiencies (> 97%) are found to be achievable in the multiwave regime. Based on available material data for silver doped arsenic sulphide glasses, the optimum parameters for operation at 632.8nm, 4μm and 10.6μm are calculated. The maximum efficiencies likely to be achieved and angular responses are evaluated.

RSRE MEMORANDUM 4121

PERFORMANCE PREDICTIONS FOR BULK CHALCOGENIDE GRATINGS PRODUCED BY THE PHOTODISSOLUTION EFFECT

C W Slinger

CONTENTS PAGE NUMBERS

1. INTRODUCTION

Chalcogenide glasses, depending upon composition, are capable of the transmission of electromagnetic radiation from the visible to beyond 15μm [1], including the atmospheric windows of 3-5μm and 8-14μm. In addition, many of them exhibit a wide variety of photoinduced phenomena. These effects include photobleaching and photodarkening, and more substantial effects such as photopolymerisation, photocrystallisation and the photodiffusion of metals [2]. Such phenomena, especially photodiffusion, in combination with the high transmission of the bulk glasses, may be useful in the production of diffractive elements for the infra-red wavebands.

Diffraction elements have several potential uses. For example, they have some advantages over conventional refractive elements (typically germanium lenses in the IR bands), particularly where weight and cost are important considerations [3]. Also, they may be used as combiners, filters and have other novel applications.

In this memo, bulk diffractive structures, capable of being produced by photodiffusion in chalcogenides, will be analysed. The treatment is limited to bulk gratings and will not consider surface relief gratings - also capable of being produced by photodissolution. A brief description of the effect is used to show how the simplest gratings to fabricate are predominantly rectangular in profile. In contrast to the sinusoidal case, not a great deal of work has been done on the properties of such gratings. A multiwave coupled wave theory is derived, capable of analysing diffraction by the rectangular gratings over a wide range of conditions. Theoretical results, derived from the model, are then presented, and the limiting cases of thin and volume (thick) diffraction discussed. The multiwave regime is then investigated by numerical solution of the coupled wave equations. Finally, the likely performance of a typical chalcogenide/photodoped metal system is determined and the required modulations and thicknesses estimated for the optimum efficiencies.

2. THE PHOTODISSOLUTION EFFECT

The following discussion is intended to give a rough, qualitative explanation of the phenomenon. For a more detailed treatment, the reader is referred to the literature [eg 2,4]

In simple terms, photodissolution (also known as photodoping) is an effect where actinic radiation causes the migration of a metal through an amorphous chalcogenide

Typically the chalcogenide may be one of those in the arsenic/sulphur system, and the metal silver or copper. A wide range of combinations using other chalcogenides and or metals are, however, possible [4]. The radiation can be over a wide band, above or below the band edge of the material. Photodissolution rates tend to increase with photon energy.

In practice, a chalcogenide film, usually formed by evaporation or spinning [5], is coated on one side of a thin metallic layer. Initially, radiation of a suitable wavelength is absorbed at the glass/metal interface. This causes growth of a metal doped region into the glass. Subsequently, the incoming radiation is absorbed at the undoped/doped glass boundary, causing further growth of this region and gradually depleting the metal reservoir. It is important to note that the migration of the metal is only along the direction of the incoming radiation - there is a distinct boundary between the undoped and the doped regions. In this way, bands of photodoped material grow into the initially undoped glass.

3. GRATING FORMATION

The photodissolution mechanism can be used to produce gratings. For example, exposure through a periodic mask will eventually produce a rectangular grating throughout the thickness of the chalcogenide film (figure 1). Holographic exposure techniques (interference of two or more wavefronts) can also be used for grating formation [6,7]. In the latter case, however, the grating structure is more complex with a varying profile through the depth of the film.

Early work on photodoping has been, to a large extent, driven by the search for very high resolution photoresists [8] (0.1 μm lines have been produced by chalcogenide resists [4]). Thus, resolution of the material is more than acceptable for gratings for visible and infrared diffractive applications.

The differing refractive indices of the photodoped and undoped regions result, in the simplest case of mask exposure, in a periodic rectangular profile refractive index modulation, throughout the volume of the material. In this way, a diffractive transmission element may be produced. Reflective, diffractive elements would require the grating planes be approximately parallel to the film surface. This would be difficult to achieve with the recording techniques outlined above. Distributing the metal as small grains throughout the film and using holographic exposure may overcome this.

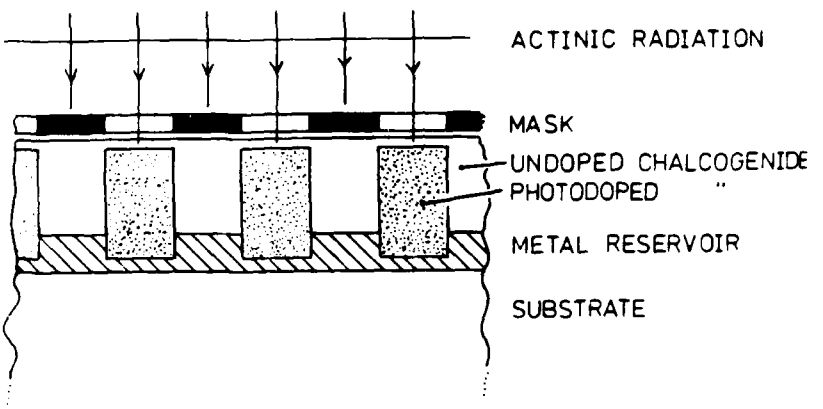

Figure 1. Production of a photodoped rectangular grating by exposure through a mask. For clarity, the metallic reservoir is shown sandwiched between the substrate and the chalcogenide. To facilitate removal of the unused metal after exposure, however, the metal is, in practice, deposited on top of the chalcogenide, and exposure made either through it, or the substrate.

Initial work is aimed at exploiting bulk rectangular transmission gratings. However, a surface relief grating can easily be obtained by selective etching of the photodoped, bulk grating [4]. Such structures will be the subject of a future analysis.

4. THEORETICAL ANALYSIS

In the following, a theoretical model, based on that of Magnusson and Gaylord [9], is derived. Using this model diffraction by bulk, rectangular profile gratings is analysed. From this, it should be possible to determine the diffraction efficiency of the grating, as a function of the grating parameters. In this way the maximum efficiency likely to be achievable and the feasibility of fabrication of the grating can be estimated.

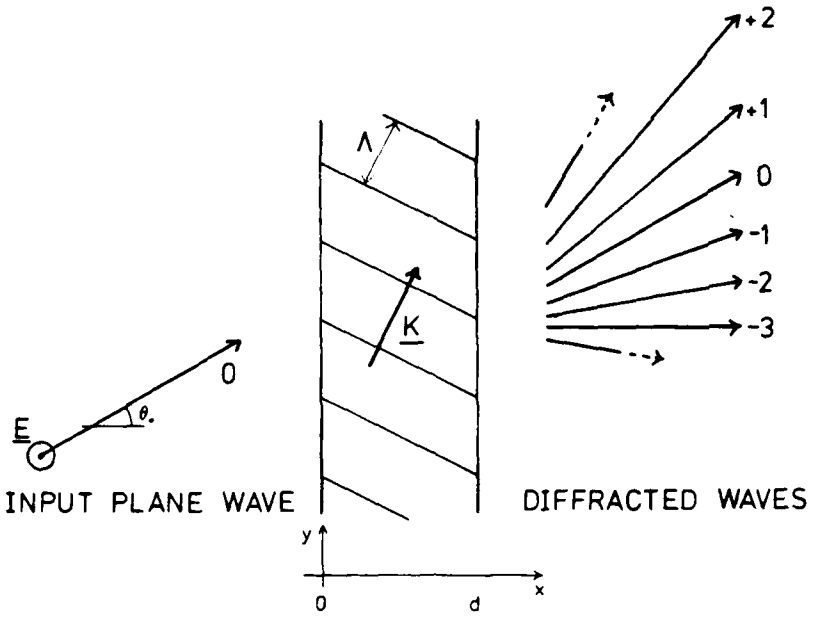

Figure 2. The grating system to be analysed.

4.1 The Coupled Wave Model

The diffractive element is bounded in an infinite, parallel sided slab. The grating characteristics in the slab will generally vary as a function of y, but is assumed to be locally plane (figure 2). This is a valid assumption if the grating vector does not change much as a function of x [10]. The modulation profile can be written as the Fourier Series:

$$\epsilon(\underline{r}) = \epsilon_o' - j\epsilon_o'' + \sum_{i=1}^{\infty} (\epsilon_i' - j\epsilon_i'') \cos(i\underline{K}.\underline{r}) \qquad (1)$$

where the profile is assumed to be an even function. For the rectangular profile:

$$\epsilon_o = \epsilon_{min} + \Delta\epsilon\ \mu$$
$$\epsilon_i = (2/i\pi)\ \Delta\epsilon\ \sin(i\mu\pi) \qquad (2)$$

where

ϵ_o' is the bulk dielectric constant of the slab

ϵ_o'' is the bulk absorption

ϵ_i' and ϵ_i'' are the phase and absorption modulation of the ith harmonic of the grating profile.

$\underline{K}$ is the grating vector, the direction of which is perpendicular to the grating fringes,

with $|\underline{K}| = 2\pi/\Lambda$, where Λ is the grating period.

and $\Delta\epsilon = \epsilon_{max} - \epsilon_{min}$

μ is a fill (mark/space) parameter.

The modulation is taken to be constant throughout the depth of the grating. Replay is assumed to be with an inifinite, monochromatic plane wave, at angle θ_o to the slab normal. The grating is taken to be index matched to the surrounding medium. The polarisation of the replay wave is assumed perpendicular to the plane of the grating - this ensures maximum coupling. The time independent, scalar wave equation can thus be used

$$\nabla^2 E + \beta^2 (\epsilon/\epsilon_o) E = 0 \qquad (3)$$

where $\beta = 2\pi/\epsilon_o'/\lambda$ is the propagation constant in the grating,

λ is the free space wavelength of the radiation.

It is assumed that the diffracted waves are such that the electric field in the grating, on replay, is in the form:

$$E = \sum_{m=-\infty}^{+\infty} A_m \exp(-j \underline{k}_m . \underline{r}) \qquad (4)$$

where A_m is the amplitude of the mth diffraction order having wave vector $\underline{k}_m$ and m = 0 corresponds to the replay wave.

A relationship between these wave vectors is taken to be in the 'k-vector closure' form:

$$\underline{k}_m = \underline{k}_o + m\underline{K} \qquad (5)$$

Substituting equation (4) into (3), with (1) and (5), and equating coefficients of $\exp(-j\underline{k}_m . \underline{r})$, gives a set of differential equations of the form:

$$\frac{d^2A_m}{dx^2} - 2jk_{mx}\frac{dA_m}{dx} + \left[\left[\beta^2 - k_m^2\right] - j\beta^2\frac{\epsilon_o''}{\epsilon_o'}\right]A_m$$

$$+ \frac{\beta^2}{2}\sum_{i=1}^{\infty}\left[\frac{\epsilon_i'}{\epsilon_o'} - j\frac{\epsilon_i''}{\epsilon_o'}\right]\left[A_{m+i} + A_{m-i}\right] = 0 \qquad (6)$$

The approximation is then made that second deriatives in (6) are negligible. This is valid if the amplitudes A_m change relatively slowly with x. From (6), it can be seen that this situation will arise if the dephasing parameter $(\beta^2-k_m^2)$, the ratio ϵ_o''/ϵ_o' and the modulation ratios ϵ_i/ϵ_o are small. The latter two conditions can be met if:

$$\epsilon_o'', \ \epsilon_i' \text{ and } \epsilon_i'' \ll \epsilon_o' \qquad (7)$$

Dropping the second derivatives, equations (6) simplify to become

$$\frac{k_{mx}}{\beta}\frac{dA_m}{dx} + (\alpha + j\nu_m)A_m + j\sum_{i=1}^{\infty}\left[\kappa_i' - j\kappa_i''\right]\left[A_{m+i} + A_{m-i}\right] = 0 \qquad (8)$$

where

$$\alpha = \frac{\beta\epsilon_o''}{2\epsilon_o'}, \quad \nu_m = \frac{(\beta^2 - k_m^2)}{2\beta},$$

and

$$\kappa_i' = \frac{\beta\epsilon_i'}{4\epsilon_o'}, \quad \kappa_i'' = \frac{\beta\epsilon_i''}{4\epsilon_o'}.$$

The physical interpretation of equations (8) is as follows: Each diffraction order A_m is coupled to the (m ± i) orders (A_{m+i} and A_{m-i}) by the ith coupling coefficeints (κ_i' and κ_i''). In contrast to the coupling mechanisms in a sinusoidal grating (i = 1 only), the coupling paths in gratings of more complex profile are much more numerous. The central terms include absorption losses (α) and the dephasing term (ν_m), a measure of the mismatch in phase velocities of the diffracted orders.

For significant power transfer from one order to another, three conditions must be met [11]. Firstly, there must be a coupling path between the two orders. Also their phase velocities must be approximately equal. Finally, the length of the

$$\frac{d^2A_m}{dx^2} - 2jk_{mx}\frac{dA_m}{dx} + \left[\left[\beta^2 - k_m^2\right] - j\beta^2\frac{\epsilon_o''}{\epsilon_o'}\right]A_m$$

$$+ \frac{\beta^2}{2}\sum_{i=1}^{\infty}\left[\frac{\epsilon_i'}{\epsilon_o'} - j\frac{\epsilon_i''}{\epsilon_o'}\right]\left[A_{m+i} + A_{m-i}\right] = 0 \qquad (6)$$

The approximation is then made that second deriatives in (6) are negligible. This is valid if the amplitudes A_m change relatively slowly with x. From (6), it can be seen that this situation will arise if the dephasing parameter $(\beta^2-k_m^2)$, the ratio ϵ_o''/ϵ_o' and the modulation ratios ϵ_i/ϵ_o are small. The latter two conditions can be met if:

$$\epsilon_o'', \ \epsilon_i' \text{ and } \epsilon_i'' << \epsilon_o' \qquad (7)$$

Dropping the second derivatives, equations (6) simplify to become

$$\frac{k_{mx}}{\beta}\frac{dA_m}{dx} + (\alpha + j\nu_m)A_m + j\sum_{i=1}^{\infty}\left[\kappa_i' - j\kappa_i''\right]\left[A_{m+i} + A_{m-i}\right] = 0 \qquad (8)$$

where

$$\alpha = \frac{\beta\epsilon_o''}{2\epsilon_o'}, \quad \nu_m = \frac{(\beta^2 - k_m^2)}{2\beta},$$

and

$$\kappa_i' = \frac{\beta\epsilon_i'}{4\epsilon_o'}, \quad \kappa_i'' = \frac{\beta\epsilon_i''}{4\epsilon_o'}.$$

The physical interpretation of equations (8) is as follows: Each diffraction order A_m is coupled to the (m ± i) orders (A_{m+i} and A_{m-i}) by the ith coupling coefficeints (κ_i' and κ_i''). In contrast to the coupling mechanisms in a sinusoidal grating (i = 1 only), the coupling paths in gratings of more complex profile are much more numerous. The central terms include absorption losses (α) and the dephasing term (ν_m), a measure of the mismatch in phase velocities of the diffracted orders.

For significant power transfer from one order to another, three conditions must be met [11]. Firstly, there must be a coupling path between the two orders. Also their phase velocities must be approximately equal. Finally, the length of the

interaction region must be correct. Note, however, that indirect coupling can occur via other diffraction orders.

Let the volume parameter Ω and the parameter P be defined as, respectively,

$$\Omega = K^2/(2\beta\kappa_1) \tag{9}$$

and

$$P = \sin(\theta_o - \Phi)\, 2\beta/K \tag{10}$$

where $\kappa_1 = \kappa_1' - j\kappa_1''$

and Φ is the grating slant (angle of the grating vector to the slab face).

On the substitution into equations (8),

$$\frac{k_{mx}}{\beta}\frac{dA_m}{dx} + \left\{\alpha - j\, m\, \kappa_1\, \Omega\, (m + P)\right\} A_m + j \sum_{i=1}^{\infty} \kappa_i \left[A_{m+i} + A_{m-i} \right] = 0 \tag{11}$$

Absorption losses are now neglected. For the chalcogenides under consideration, this is a good approximation over much of their transmission band. For example, amorphous As_2S_3 has an absorption coefficient α of around 10^{-2} cm^{-1} in the 1 to 10μm band [12]. The photodoped regions, depending on composition, may be slightly more absorbing (due to some photodarkening). Note that the grating structures of interest are of the order of tens of microns in thickness. The assumption of no absorption also precludes the existence of absorption modulation.

Finally, the grating is assumed to be unslanted, ie the grating vector is parallel to the input and exit boundaries. Such gratings would result, for example, using a mask with exposure by plane wave, normally incident radiation. Thus the problem becomes one of analysing a pure phase, lossless, unslanted, transmission grating. Equations (10) then reduce to the set of coupled equations, for $m = -\infty,\ldots,-1,0,+1,\ldots,+\infty$:

$$\frac{dA_m}{d\xi} - j\, m\, \Omega\, (m + P)\, A_m + j \sum_{i=1}^{\infty} \frac{\kappa_i}{\kappa_1} \left[A_{m+i} + A_{m-i}\right] = 0 \tag{12}$$

where $\xi = \kappa_1' x/\cos\theta_o$ is the modulation parameter.

These equations obey power conservation. The transmission grating boundary conditions are:

$$A_m(x = 0) = 0 \qquad (m \neq 0)$$

$$\text{and} \quad A_o(x = 0) = 1 \tag{13}$$

Solution of equations (12) subject to these boundary conditions will give the amplitudes of the diffraction orders, A_m, as a function of the modulation ξ, for a given Ω and P.

4.2 Diffraction Regimes

In general, the solution of the infinite set of equations (12) requires numerical techniques and truncation to a finite number of diffraction orders. However, there are two limiting cases for which analytic solutions are possible. These are at opposite extremes of transmission grating behaviour, and occur when the thickness parameter Ω takes vanishingly small or very large values. The former case is referred to thin grating behaviour (often termed Raman Nath Diffraction after Raman and Nath's thin, sinusoidal grating analysis [13]); the latter as volume (or thick) diffraction.

Thin Grating. As Ω tends to very small values, the dephasing term for each diffraction order becomes very small. Large numbers of orders can have significant power in them (this can be seen qualitatively from figure 3), and equations (12) reduce to, for $m = -\infty,\ldots,-1,0,+1,+2,\ldots,+\infty$:

$$\frac{dA_m}{d\xi} + j \sum_{i=1}^{\infty} \frac{\kappa_i}{\kappa_1} \left[A_{m+i} + A_{m-i} \right] = 0 \tag{14}$$

For the sinusoidal case ($\kappa_i = 0$ for $i \neq 1$) the solution is well known, and is in terms of Bessel functions:

$$A_m(\xi) = (-j)^m J_m(2\xi) \tag{15}$$

where $J_i(x)$ is a Bessel function of the first kind, of order i. A thin, sinusoidal phase grating is unselective, having a maximum efficiency η_m of 33.9%, for $m = \pm 1$ at $\xi = 1.84$, where η_m is defined as the ratio of power in the mth diffraction order to that in the incident, zeroeth order. This low efficiency,

combined with the large number of significant orders, generally exclude such gratings from use in many applications (although there are exceptions).

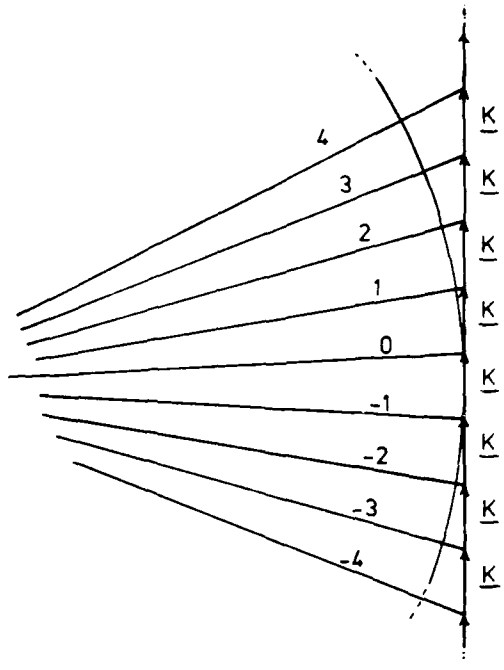

Figure 3. Ewald sphere (radius β), representation of diffraction by a sinusoidal grating with some 'thin' behaviour. Many diffraction orders are significant due to the small size of the dephasing parameters ν_m.

For the thin, rectangular grating case, with the modulation as specified by equation (2), then [14]:

$$\eta_o = |A_o(\zeta)|^2$$

$$= 1 - 4(\mu - \mu^2).\sin^2\{\pi\zeta/(2\{1 - \cos(2\pi\mu)\})^{\frac{1}{2}}\} \qquad (16)$$

$$\eta_m = |A_m(\zeta)|^2$$

$$= \{2/(m\pi)^2\}\{1 - \cos(m2\pi\mu)\}.\sin^2\{\pi\zeta/(2\{1 - \cos(2\pi\mu)\})^{\frac{1}{2}}\} \quad (m\neq 0)$$

Maximum efficiency is 40.5% for the ± 1 orders. As in the sinusoidal case, such thin, rectangular phase gratings have, generally, limited use in diffractive elements (computer generated holograms are often of this type, but in their case, efficiency can be increased by copying into a volume medium).

The thin grating regime is found, typically, for $\Omega \leqslant 0.01$. As Ω increases much above this value, then equations (13) become less accurate, as the dephasing terms start to become significant.

Volume Grating. At large values of Ω, Bragg effects become dominant. Diffraction orders, other than the on-Bragg order, have such a large mismatch in phase velocities that very little power is coupled to them. This is illustrated in figure 4. In the limiting case then, for replay of the grating in the vicinity of the m = i on-Bragg condition, the infinite set of coupled wave equations (12) reduce to only two in number - provided 'i' is a harmonic of the grating profile:

$$\frac{dA_o}{d\xi} + j \frac{\kappa_i}{\kappa_1} A_i = 0$$

and

$$\frac{dA_i}{d\xi} - j\, i\, \Omega\, (i + P)\, A_i + j \frac{\kappa_i}{\kappa_1} A_o = 0 \qquad (17)$$

Analytic solutions are possible. When fully on Bragg, these reduce to:

$$\eta_o = \cos^2(\xi\, \kappa_i/\kappa_1)$$

and

$$\eta_i = \sin^2(\xi\, \kappa_i/\kappa_1) \qquad (18)$$

The solutions in (18) agree with Kogelnik's analysis [15], when i = 1. Thus, for large enough Ω, 100% conversion to the ith order is achievable. This occurs when replay is on Bragg for the ith harmonic of the grating, at:

$$\xi = (2n + 1)\pi\, \kappa_1/2\kappa_i \qquad (n = 0,1,2,3,\ldots) \qquad (19)$$

The high efficiencies of these volume, phase gratings mean that they have many applications. In particular, they find use in diffractive optical elements - eg supermarket scanners, head-up displays. To the author's knowledge, all the bulk grating volume elements use sinusoidal modulation. This is because most practical

recording media respond in this way. However, as seen above, there is no reason why volume, rectangular gratings cannot be used to similar effect.

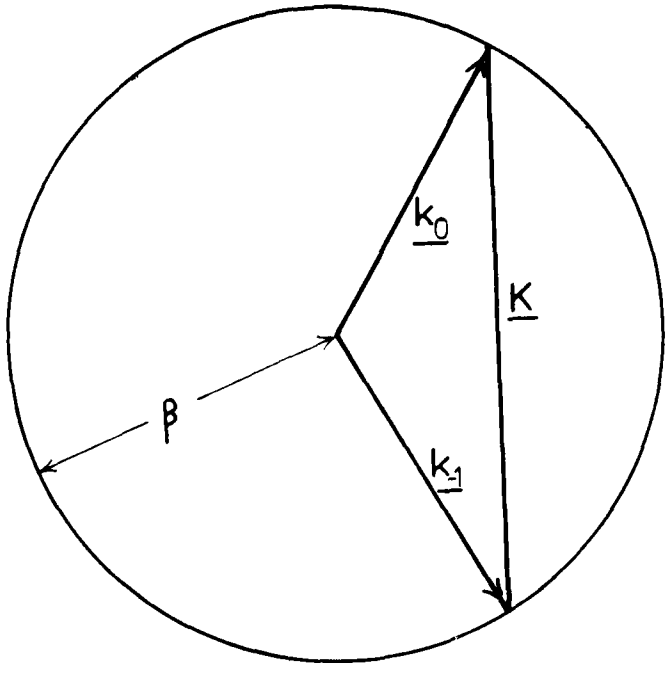

Figure 4. Ewald sphere representation of diffraction by a grating with significant volume behaviour. Only the zero and first diffraction orders are present. Other orders do not carry significant power as ν_m ($m \neq -1$) are too large.

Multiwave Grating. Between thin and volume regimes, there is an intermediate region of grating behaviour. In practice, many gratings may not have large enough values of Ω to guarantee that they will operate in the volume region. Investigation of the multiwave regime is therefore necessary to determine if acceptable grating behaviour is possible. For example, it may be feasible to achieve high enough efficiencies, for a particular application, without wasting unnecessary effort to increase the Ω value of the grating.

In the multiwave regime, the number of significant diffraction orders is generally large but finite. Recourse to numerical solution of a truncated set of equations (12) is therefore necessary. Thus, for $m = -N,....-1,0,+1,....N$:

$$\frac{dA_m}{d\xi} - j\, m\, \Omega\, (m + P)\, A_m + j \sum_{i=1}^{2N} \frac{\kappa_i}{\kappa_1} (A_{m+i} + A_{m-i}) = 0 \qquad (20)$$

where N is the number of the highest diffraction order containing significant power. Generally speaking, if Ω is small, N will be large and as Ω increases, N will decrease accordingly. This reflects the grating's performance as it changes between the two limiting cases of thin and volume behaviour.

5. NUMERICAL RESULTS

The coupled wave equations (20), subject to the boundary conditions (13), were solved using a Runge Kutta technique. The diffracted amplitudes from various grating profiles were calculated as a function of the thickness parameter Ω and the modulation ν, for on-Bragg replay of the first diffraction order.

The following grating profiles were investigated in some detail:

i) Sinusoidal
ii) Rectangular, with the fill parameter, equation (2), $\mu = 0.1$
iii) Rectangular, $\mu = 0.25$
iv) Rectangular, $\mu = 0.5$
v) Rectangular, $\mu = 0.75$
vi) Rectangular, $\mu = 0.9$.

The sinusoidal case ($\kappa_i = 0$, $i \neq 1$) is the simplest. It is included to investigate the relative merits of sinusoidal and rectangular modulation gratings - a question of importance for a wide range of grating applications. Case (iv) corresponds to a square wave grating.

The results of the analyses are shown in Figures 5 to 10, in the form of contour plots. The height of the contours represent the efficiency of diffraction into the +1 order (η_1). Note the logarithmic scale for the thickness parameter Ω. Figures 11 and 12 show perspective views of the efficiency variation for the sinusoidal and square wave cases respectively.

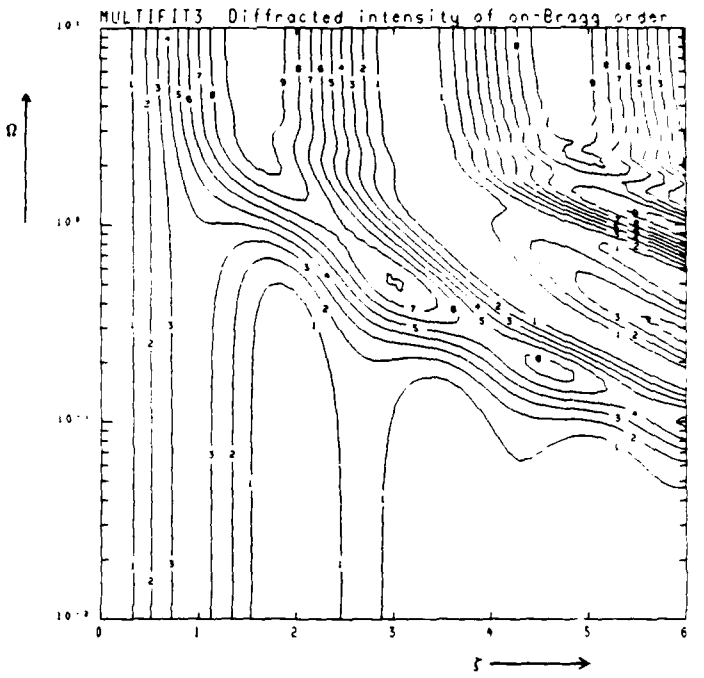

Figure 5. Sinusoidal grating. +1 diffracted intensity as a function of the modulation parameter ξ and the volume parameter Ω. The height of the contour is proportional to the diffracted efficiency. Contour 1 = 10%, 2 = 20% etc.

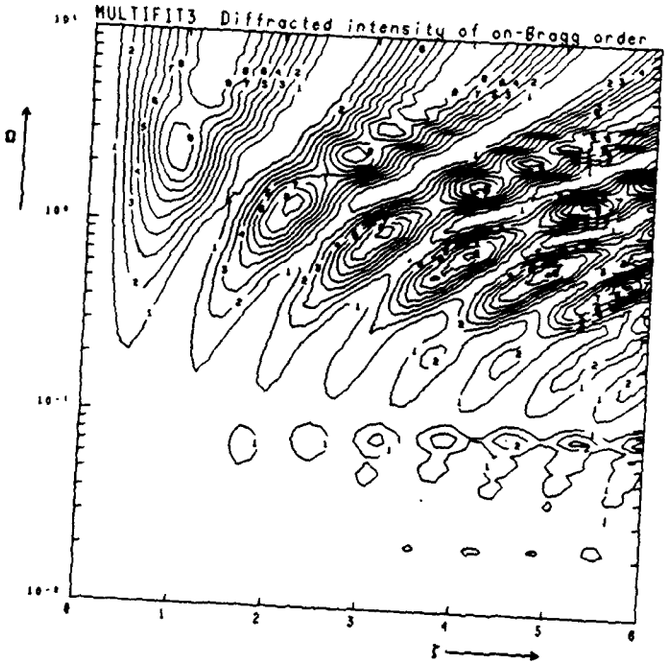

Figure 6. Rectangular grating, $\mu = 0.1$. Otherwise, as in Figure 5.

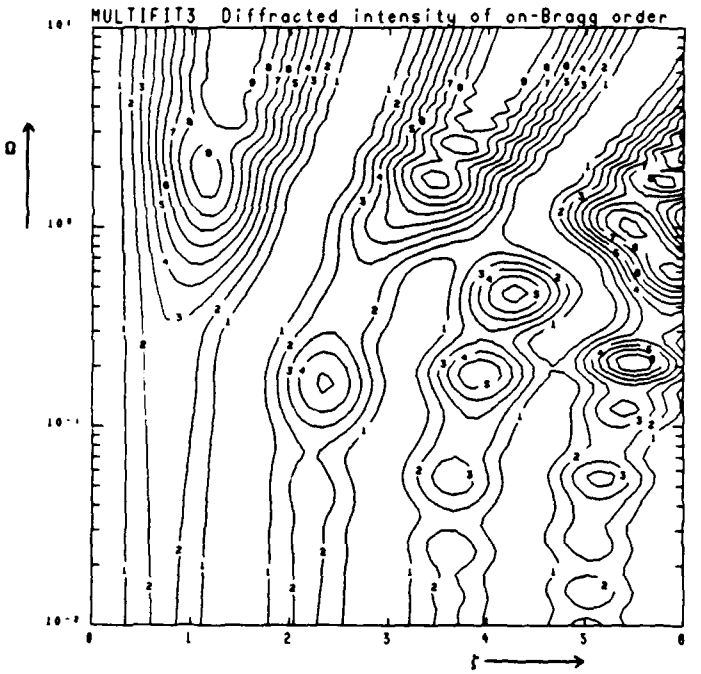

Figure 7. Rectangular grating, μ = 0.25. Otherwise, as in Figure 5.

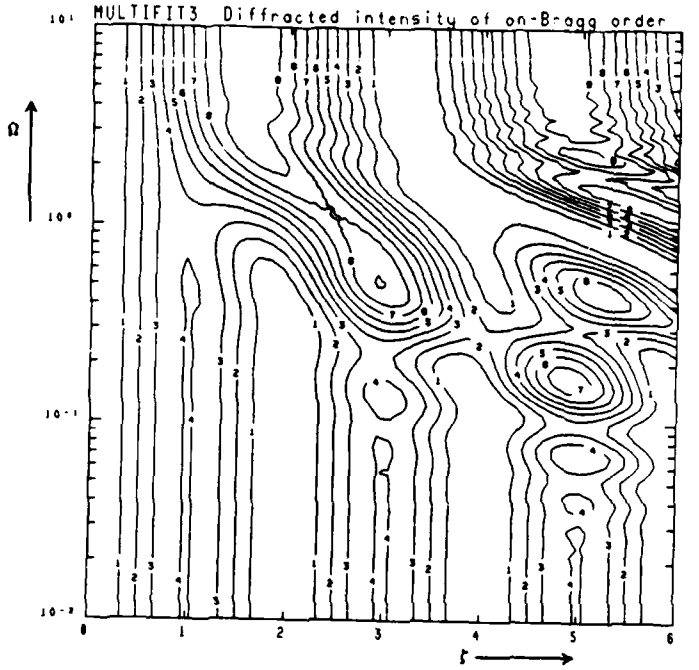

Figure 8. Rectangular grating, μ = 0.5. Otherwise, as in Figure 5.

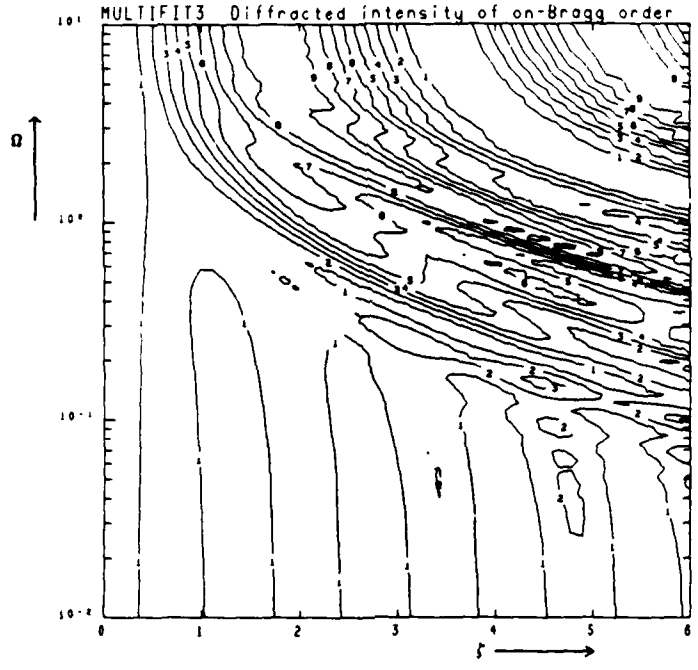

Figure 9. Rectangular grating, μ = 0.75. Otherwise, as in Figure 5.

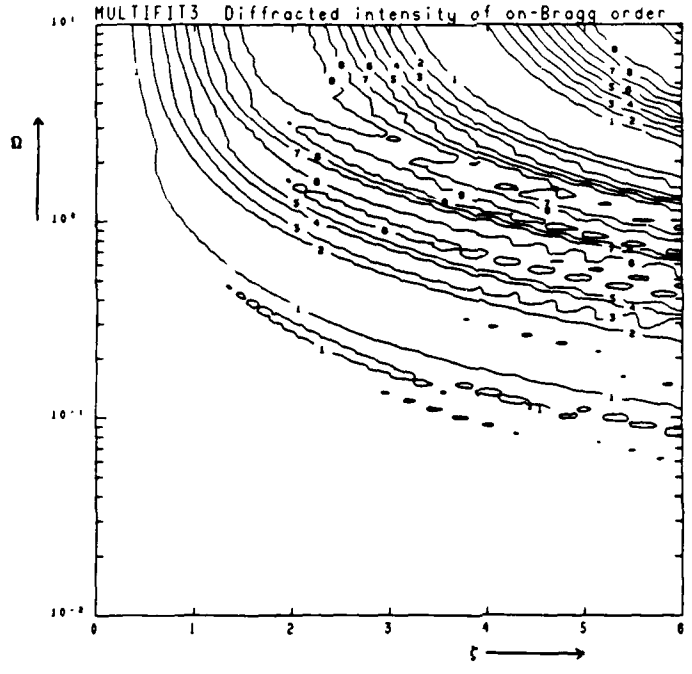

Figure 10. Rectangular grating, μ = 0.9. Otherwise, as in Figure 5.

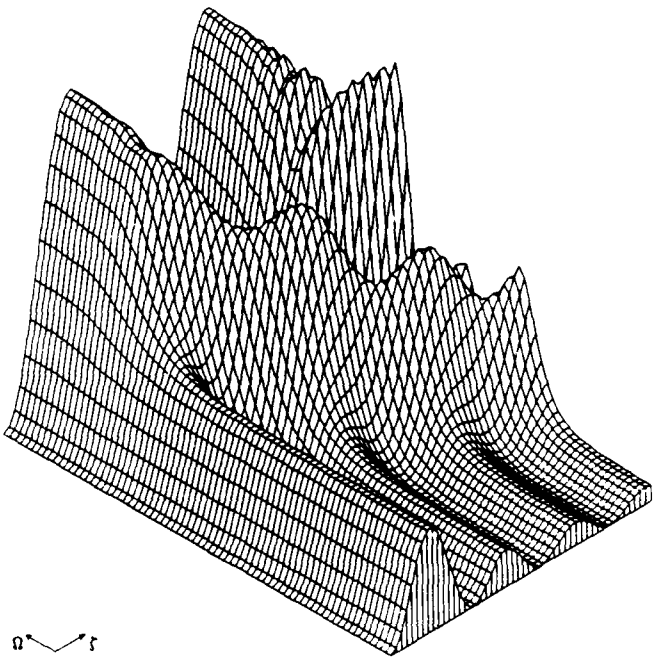

Figure 11. Perspective view of Figure 5 (sinusoidal grating).

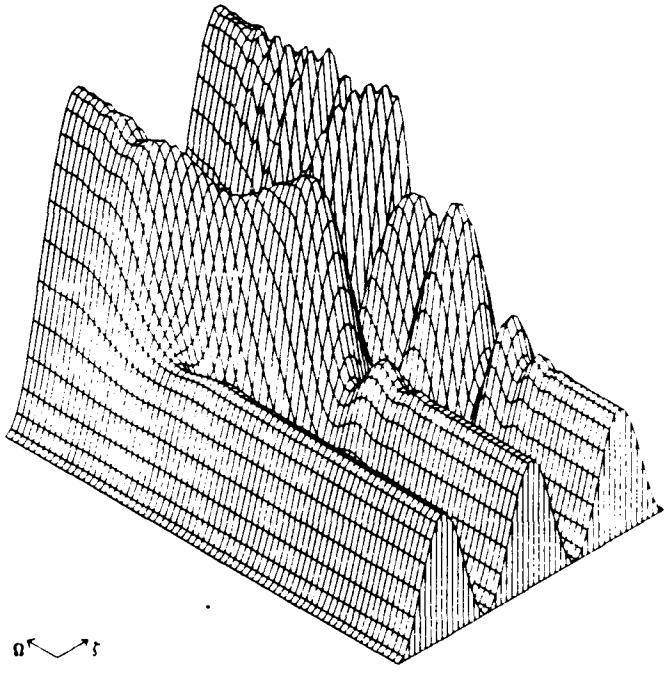

Figure 12. Perspective view of Figure 8 (square wave grating).

5.1 Analysis of Results

Several observations can be made from the plots.

i) For low values of Ω, in all cases, the results agree closely with the appropriate analytic expressions (equations (15) and (16)) for thin grating behaviour.

ii) At high values of Ω, the diffraction efficiencies all converge to the same values, irrespective of the grating profile. These values are those derived for the volume sinusoidal case, given by equations (18) and (19). This seems a reasonable result and can be explained by noting that the diffraction orders, other than the ± 1, are so far off Bragg that there is no power coupled in to them. Thus the behaviour of all grating profiles converges to the sinusoidal case under these conditions.

iii) High efficiencies in all cases can occur in several areas in the multiwave regime - for example, over 91% at $(\xi,\Omega) = (2.97,0.5)$ for the square wave profile ($\mu = 0.5$). This can be important for practical devices in that gratings can be fabricated that are not 'volume', yet are of high efficiency. This enables a much wider choice in grating thickness, modulation, and grating vector size. The lower the value of Ω required, for example, the less off-axis a transmissive, diffractive element would have to be.

iv) In terms of the maxima of the diffraction efficiency η_1, the square wave grating is equal or superior to the sinusoidal case. This is true in the thin, multiwave and volume regions. Thus square wave modulation should not be regarded as a limitation in a bulk modulated recording medium.

v) There is a progression in the efficiency characteristics of the rectangular gratings with increasing μ. At low values of μ, the size of the modulation ξ for high efficiency in the multiwave regime is small. As μ increases, so does the required modulation ξ. In the table below, the minimum modulations for the first peak in η_1 over 90% are shown with various ξ. Ω values for these peaks are also listed.

TABLE 1

μ	0.05	0.10	0.25	0.30	0.35	0.40	0.45	0.50
ξ	0.88	0.92	1.147	1.34	1.43	1.46	1.53	$\pi/2$
Ω	2.3	2.2	2.0	3.9	3.5	3.3	2.9	4.9

6. SIGNIFICANCE OF THE RESULTS IN RELATION TO THE PHOTODOPED AsS SYSTEM

In this section the numerical results will be considered in the light of the known physical properties of the photodoped chalcogenides. The optimum grating structure will be calculated, and the required physical grating parameters (thickness, frequency, etc) estimated. Practical grating efficiency will be predicted.

Two cases will be considered. These will be gratings designed for operation at 632.8nm and at 10.6μm. The former corresponds to the HeNe laser line. Gratings at this wavelength will be easy to assess and characterise. The latter is the CO_2 laser line, and lies near the centre of the 8–14μm infra-red atmospheric window.

The refractive indices of the undoped and photodoped materials depend on the composition of the As_xS_{1-x}. This can be varied over a wide range. For $As_{30}S_{70}$ photodoped with silver, the following values have been reported [16]:

	Undoped	Photodoped
Refractive index at 632.8nm	2.36	2.71
Refractive index at 10.6μm	2.22	2.42

These figures are preliminary. Detailed material characterisation is currently underway.

6.1 Validity of the Theoretical Analysis

An important step in the derivation of equations (20) was the neglect of second derivatives. The validity of this assumption depends on the ratio of the first

harmonic phase modulation to the bulk dielectric constant (ie, ϵ_1'/ϵ_0'). The smaller this quantity, the more accurate the assumption. From equations (2)

$$\frac{\epsilon_1'}{\epsilon_0'} = \frac{2\,\Delta\epsilon\,\sin(\mu\pi)}{\pi\,(\epsilon_{min} + \Delta\epsilon\,\mu)} \qquad (21)$$

This expression is a maximum (equivalent to the worst case) when μ is given by:

$$\pi\,(\epsilon_{min}/\Delta\epsilon + \mu) - \tan(\mu\pi) = 0 \qquad (22)$$

Solving this gives a maximum of ϵ_1'/ϵ_0' at 632.8nm of 0.176 (μ = 0.472) and of 0.110 (μ = 0.483) at 10.6μm.

According to a rigorous analysis of a sinusoidal grating [17], a value of ϵ_1'/ϵ_0' = 0.12 gives less than 1% error on η_1 for Ω = 2 and negligible error for Ω = 10. Thus, for the material in question, neglect of second derivatives is likely to be a valid approximation.

It is appropriate here to digress briefly, and consider a surface relief, as opposed to bulk, rectangular grating. At 632.8mn, maximum ϵ_1'/ϵ_0' = 1.13 (μ = 0.310) and at 10.6μm, maximum ϵ_1'/ϵ_0' = 1.02 (μ = 0.32). Thus, prediction of η_1 for surface relief, photodoped gratings, requires second order theory.

6.2 Minimisation of Grating Thickness

One practical problem associated with photodoping is concerned with grating thickness. This is for two reasons. Firstly, a layer of suitable thickness must be evaporated or spun onto a supporting substrate. Thicknesses of greater than a few hundred nanometers are more awkward in this respect. More significantly however, the rate of migration of the photodoped region through the chalcogenide layer is relatively slow. Migration rates vary considerably, depending upon metal [18] and chalcogenide composition [19], the wavelength of the actinic radiation and its intensity [20]. If the thickness requirements for the grating are too large, migration time will be large, and holographic exposure would require a very stable environment. Mask exposure would circumvent stability problems, but long exposure times would still increase costs.

The thickness of the photodoped layer d, is related to the exposure time t by

$$d \simeq k\,\sqrt{t} \qquad (23)$$

where k is a rate constant. For an intensity of 75 mW cm^{-2}, from a tungsten lamp, and silver doping of $As_{33}S_{67}$, k = 0.015μm $s^{-\frac{1}{2}}$ [19]. k increases rapidly with decreasing wavelength.

For the above reasons, minimisation of grating thickness is of prime importance. From the numerical calculations, it was seen that the required modulation ζ for high efficiency, decreased with decreasing μ. Since

$$\zeta = \frac{\kappa_1' d}{\cos \theta_o} \tag{24}$$

it might be thought that a low value of ζ would minimise d, the grating thickness. However, κ_i is also a function of μ. Rearranging (24) and using (2) gives

$$d = \frac{\lambda \cos \theta_o}{(\Delta\epsilon)^{\frac{1}{2}}} \zeta \frac{(\epsilon_{min}/\Delta\epsilon + \mu)^{\frac{1}{2}}}{\sin (\mu\pi)} \tag{25}$$

Let

$$d \propto d' = \cos \theta_o \zeta \frac{(\epsilon_{min}/\Delta\epsilon + \mu)^{\frac{1}{2}}}{\sin (\mu\pi)} \tag{26}$$

In the table below d' is calculated, using the above equation and the results from Table 1.

TABLE 2

μ value	0.05	0.1	0.3	0.35	0.4	0.45	0.5
d' at 632.8nm	10.00	5.31	2.96	2.88	2.79	2.84	2.83
d' at 10.6μm	12.99	6.90	3.83	3.74	3.59	3.65	3.66

From the table, minimum d' occurs at about μ = 0.4, for both wavelengths. This value of μ should, therefore, be used to minimise the required grating thicknesses. However, the variation in d' with μ is slight for μ = 0.35 to 0.5. Any value in this range should be acceptable.

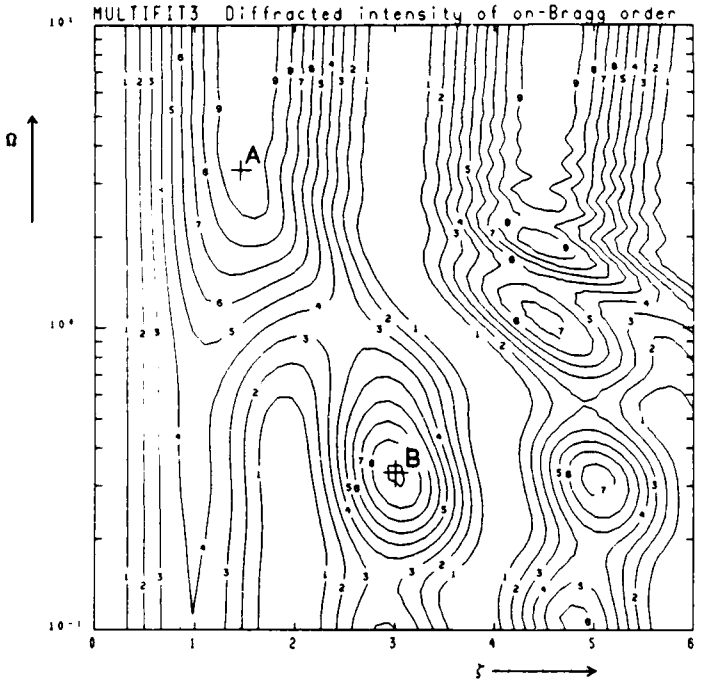

Figure 13. Contour plot for the diffraction efficiency for rectangular grating μ = 0.4 case. This corresponds to the near optimum value of μ required to minimise grating thickness. The two potential operating points, A and B, are shown.

6.3 Physical Parameters and the Predicted Performance of the Gratings

Bearing in mind the requirement for high efficiency and for the physical thickness of the grating to be a minimum, several options are available. These can be seen with the aid of figure 13 which shows a region of the ξ,Ω,η_1 contour plot for μ = 0.4. Operation in the volume regime ($\Omega \sim 10$ or greater) is a conventional choice for diffraction elements. Here, near 100% efficiency is achievable. An alternative to this is operating at one of the maxima in the multiwave regime. These options will be evaluated and compared.

Multiwave regime operation. A suitable 'operating point' (labelled 'A'), in the multiwave regime, occurs at ξ = 1.46, Ω = 3.30. At this position, an efficiency of

greater than 97% is possible. Using equations (2) and (9), the grating constants can be specified fully. The parameters for operation at a wavelength of 4μm are also shown:

TABLE 3

Parameter	ϵ_0'	ϵ_1'	κ_1'/m^{-1}	K/m^{-1}	$\Lambda/\mu m$	$\theta/^\circ$	$d/\mu m$
λ=632.8nm	6.28	1.07	1.06E6	13.2E6	0.475	15.41	1.32
4.0μm	5.30	0.562	95.8E3	1.51E6	4.15	12.07	14.90
10.6μm	5.30	0.562	36.2E3	570E3	11.01	12.07	39.5

The grating period of 0.475μm for the 632.8nm case is close to the limits of mask exposure technology, so a holographic recording technique might be more applicable. Conversely, the 4.0 and 10.6μm cases are certainly promising candidates for mask exposure, although it remains to be seen whether the exposure times for the thicknesses required by them will be acceptably short.

However, there are alternative operating points that could be of use for the 632.8nm grating. One of particular interest occurs at ξ = 3.02, Ω = 0.319 (labelled 'B' in the figure), with a peak efficiency of 92%. Again, this is the multiwave regime. Since Ω is lower for this point, the grating period will be increased, although at the expense of a corresponding increase in thickness. Operation at IR wavelengths for this point is not advantageous, as the grating periods are already large (Table 3) and any further increase in thickness would be highly undesirable. The parameters calculated for replay at 632.8nm, at B, are shown below.

TABLE 4

Parameter	ϵ_0'	ϵ_1'	κ_1'/m^{-1}	K/m^{-1}	$\Lambda/\mu m$	$\theta/^\circ$	$d/\mu m$
λ=632.8nm	6.28	1.07	1.06E6	4.11E6	1.530	4.735	2.85

It can be seen that there is a reduction in the resolution requirements of over a factor of 3, at the expense of a roughly doubling the required thickness.

Volume regime operation. At large values of Ω ($\sim$ 10 or greater), the analytic solutions to the coupled wave equations can be used to predict the required grating

parameters. 100% efficiency first occurs when (equation 19):

$$\frac{k_1' d}{\cos \theta_o} = \frac{\pi}{2} \qquad (27)$$

Combining this with the definition of the volume parameter Ω (equation (9)), yields the relation, for on-Bragg replay:

$$\frac{d}{\lambda} = \frac{\Omega n \cos \theta_o}{8 \sin^2 \theta} \qquad (28)$$

where θ is the replay angle, measured in air, and θ_o is the internal Bragg angle. Thus the normalised grating thickness d/λ is large for small replay angles, but decreases rapidly as the Bragg angle increases. Equation (28) is shown plotted in figure 14.

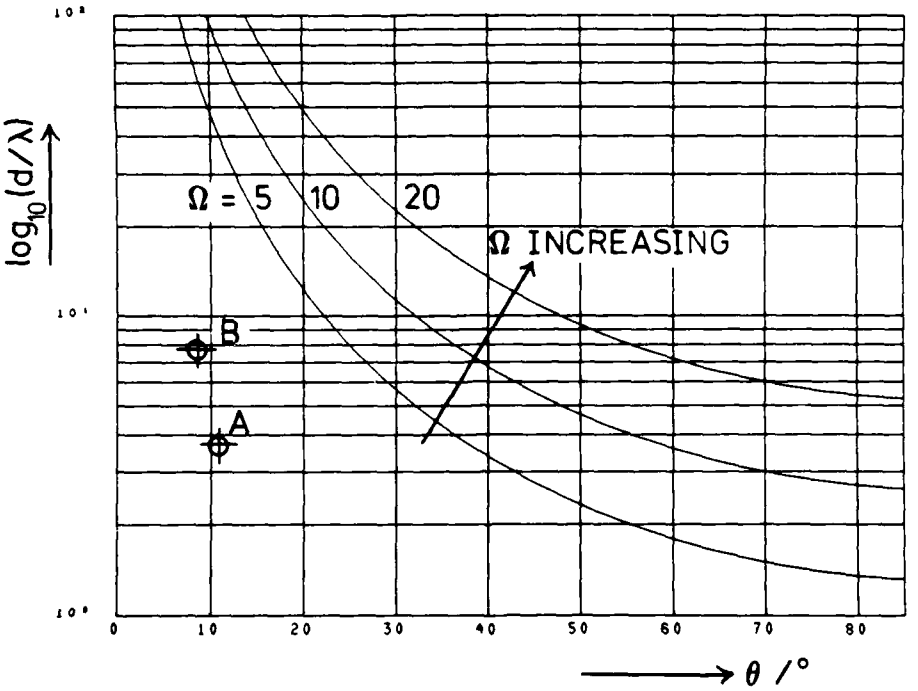

Figure 14. Variation of the normalised grating thickness d/λ as a function of the on-Bragg replay angle θ, measured in air. Volume replay (continuous curves) is compared with multiwave replay (A and B). Refractive index n is assumed to be 2.32.

A comparison of the grating thicknesses in the multiwave and volume regimes can now be made. The plot clearly shows that, if large replay angles can be tolerated ($> 60^{\circ}$), then volume regime behaviour is preferable. If smaller incident angles are required, then operation in the multiwave regime is necessary. Such considerations will be important, for example, in deciding how far off-axis a diffractive lens would operate.

6.4 Angular Response

It has been shown above, that at both the operating points A and B and in the volume region (figure 13), diffraction efficiencies of greater than 90% should be achievable. So far, the emphasis has been placed on high efficiency for minimum physical thickness. Depending upon the application, other factors may be important. One of these is the behaviour of the grating when it is off the Bragg condition, due to a move away from the design replay angle and/or wavelength. For a volume grating, the efficiency will fall, as the power in the ith on-Bragg order decreases. However no other orders, other than the zero and the ith, will be present.

This contrasts with the behaviour of non-volume gratings, where many diffraction orders can have significant amplitudes when off-Bragg replay occurs. These other orders may be highly undesirable, due to their ability to give spurious foci or images, for example.

To illustrate the presence of such orders, calculations were performed, simulating off-Bragg replays by angular dephasing. Figures 15 and 16 show the theoretical output intensities from non-volume gratings, under index matched conditions, as a function of the replay wave angle. The first figure corresponds to operating point A, at 10.6μm, the second at operating point B, at 632.8nm. In both cases, the peak in the +1 diffracted intensity corresponds to replay being on-Bragg. Either side of this angle, the gratings become increasingly off-Bragg, and the efficiency falls. It can be seen that the former (case A) is more of a volume response, in that the number of significant diffraction orders is relatively small. Conversely, in the latter case (B), more orders are significant. This would be expected, as at B the lower value of Ω (0.319 compared to 3.30) results in a grating with less volume character.

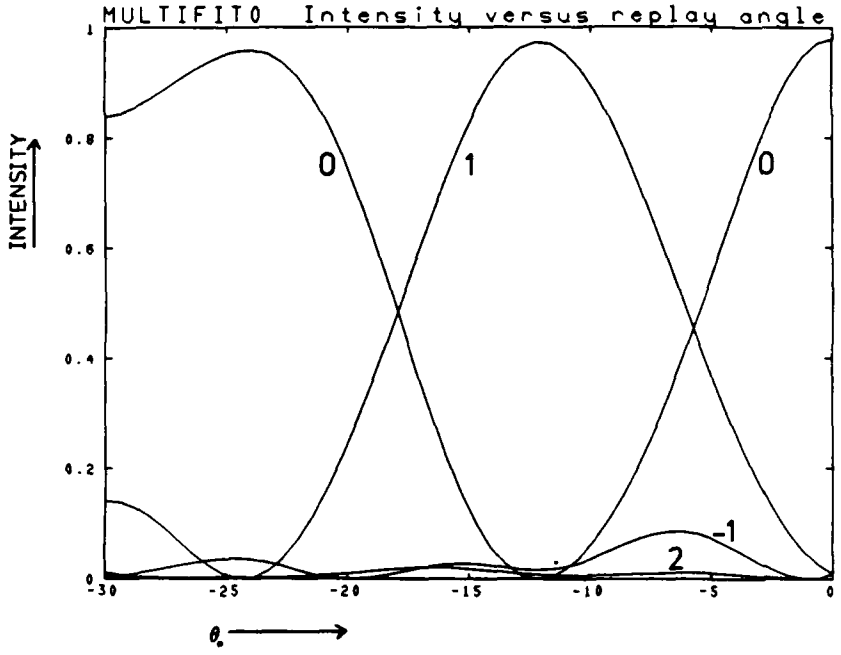

Figure 15. Angular response of a grating operating at A (Figure 13) at 10.6μm. Diffraction intensities are plotted as a function of replay angle θ_O, measured in degrees.

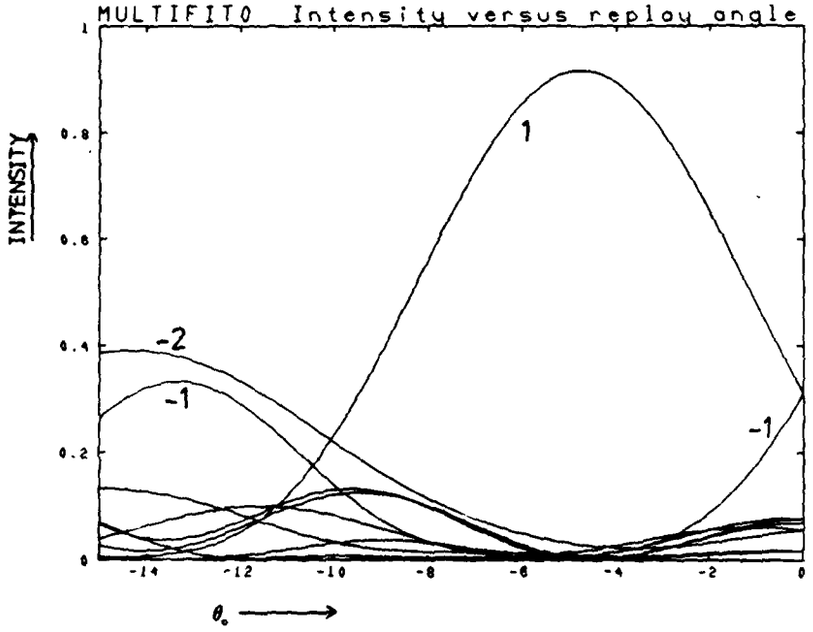

Figure 16. As in Figure 14, but operating at point B and 632.8*nm*.

7. CONCLUSION

It has been shown that the photodoping of chalcogenides may be capable of producing high efficiency transmission gratings. Such structures may be produced by mask or holographic exposure and require few fabrication steps. Bulk rectangular, phase gratings (as would be produced by mask exposure) were analysed using a coupled wave model.

For the first time, the thin, multiwave and volume diffraction regimes of such gratings have been investigated in some detail. Rectangular gratings were shown to be capable of high efficiencies (> 90%). Choice of operating point was shown to depend on angle, resolution and thickness considerations. The importance of minimising the physical thickness of the gratings was discussed and a mark/space value of $\mu = 0.4$ was found to be near optimum for this purpose. In this case, efficiencies of greater than 97% (neglecting reflection losses) were found to be possible, in both volume and multiwave regimes. The grating parameters, based on the supplied material properties of the silver doped arsenic sulphide chalcogenide glasses, were calculated for optimum operation at the wavelengths of 632.8nm, 4μm and 10.6μm.

It remains to be seen whether the required thicknesses of gratings make fabrication a practical proposition. This work is currently underway. Surface relief analogues may prove to be an attractive alternative. These are also being investigated.

In conclusion, the excellent transmission characteristics (red to far infrared), and the ease of grating fabrication, must make photodoped chalcogenides one of the prime contenders for infrared diffractive elements.

ACKNOWLEDGEMENTS

The author wishes to thank Dr Richard Home of RSRE for his encouragement and helpful discussions, and in addition, Dr Peter Ewen and Nasser Zakery of Edinburgh University for supplying the material parameters.

REFERENCES

[1] J. A. Savage "Infrared optical materials and their antireflection coatings", Adam Hilger (1985).

[2] A. E. Owen, A. P. Firth, P. J. S. Ewen "Photo-induced structural and physico-chemical changes in amorphous chalcogenide semiconductors", Philosophical Magazine B 52 No 3, pp 347-362 (1985).

[3] D. H. Close "Holographic optical elements", Optical Engineering 14 No 5, pp 408-419 (1975).

[4] A. P. Firth, P. J. S. Ewen, A. E. Owen, C. M. Huntley "Inorganic resists based on photo-doped As-S films", SPIE Advances in resist technology and processing II 539 pp 160-165 (1985).

[5] G. C. Chern, I. Lauks "Spin-coated amorphous chalcogenide films", Jrnl Applied Physics 53 No 10, pp 6979-6982 (1982).

[6] M. I. Kostyshin, E. P. Krasnojonov, V. A. Makev, G. A. Sobolev "The use of light sensitive semiconductor-metal systems for holographic applications", Applications of holography, Proceedings of the international symposium of holography, ed by J.-Ch. Vienot, J. Bulabois, J. Pasteur (Univ Besancon, France 1970) paper 11.7.

[7] S. A. Keneman "Hologram storage in arsenic trisulfide thin films", Applied Physics Letters 19 No 6, pp 205-207 (1971).

[8] E. Hajto, G. Zentai "Submicron resolution amorphous chalcogenide optical grid", Jrnl. of Non-Crystalline Solids 90, pp 581-584 (1987).

[9] R. Magnusson, T. K. Gaylord "Analysis of multiwave diffraction of thick gratings", Jrnl. Optical Society America 67 No 9, pp 1165-1170 (1977).

[10] R. R. A. Syms, L. Solymar "Localised one-dimensional theory for volume holograms", Optical and Quantum Electronics 13, pp 415-419 (1981).

[11] L. Solymar, D. J. Cooke "Volume holography and volume gratings", Academic Press, Chapter 5 (1981).

[12] P. A. Young "Optical Properties of vitreous arsenic trisulphide", Jrnl. Physics C: Solid State Physics 4, pp 93-106 (1971).

[13] C. V. Raman, N. S. Nagandra Nath "The diffraction of light by high frequency sound waves", Parts I, II, IV, V. Proc. Indian Academy Sciences 2, pp 406-412, pp 413-420, 3 pp 75-84, pp 119-125, pp 459-465 (1935-6).

[14] R. Magnusson, T. K. Gaylord "Diffraction efficiencies of thin phase gratings with arbitrary grating shape", Jrnl. Optical Society America 68 No 6, (1978).

[15] H. Kogelnik "Coupled wave theory for thick hologram gratings", Bell Systems Technical Jrnl. 48 pp 2909-2947 (1969).

[16] N. Zakery, P. J. S. Ewen, Private Communication, in connection with Research Agreement No 2087/30/RSRE.

[17] M. G. Moharam, T. K. Gaylord "Rigorous coupled wave analysis of planar grating diffraction", Jrnl. Optical Society of America 71 No 7, pp 811-818 (1981).

[18] H. Mizuno "Photo- and thermal-diffusions of metal into As_2S_3 glass", Solid State Communications 12, pp 999-1001 (1973).

[19] P. J. S. Ewen, A. Zakery, A. P. Firth, A. E. Owen "Optical monitoring of photodissolution kinetics in amorphous As-S films" paper accepted for publication in Philosophical Magazine B.

[20] T. Yaji, S. Kurita "Photodoping sensitivity of Ag into amorphous As_2S_3 films", Jrnl. Applied Physics 54 No 2, pp 647-651 (1983).

DOCUMENT CONTROL SHEET

Overall security classification of sheet ...UNCLASSIFIED.....

(As far as possible this sheet should contain only unclassified information. If it is necessary to enter classified information, the box concerned must be marked to indicate the classification eg (R) (C) or (S))

1. DRIC Reference (if known)	2. Originator's Reference	3. Agency Reference	4. Report Security Classification
	Memorandum 4121		UNCLASSIFIED

5. Originator's Code (if known)	6. Originator (Corporate Author) Name and Location
778400	Royal Signals and Radar Establishment St Andrews Road, Malvern, Worcestershire WR14 3PS

5a. Sponsoring Agency's Code (if known)	6a. Sponsoring Agency (Contract Authority) Name and Location

7. Title
PERFORMANCE PREDICTIONS FOR BULK CHALCOGENIDE GRATINGS PRODUCED BY THE PHOTODISSOLUTION EFFECT

7a. Title in Foreign Language (in the case of translations)

7b. Presented at (for conference papers) Title, place and date of conference

8. Author 1 Surname, initials	9(a) Author 2	9(b) Authors 3,4...	10. Date	pp. ref.
Slinger C W			1988.02	35

11. Contract Number	12. Period	13. Project	14. Other Reference

15. Distribution statement
Unlimited

Descriptors (or keywords)

continue on separate piece of paper

Abstract
Gratings produced by the photodoping of chalcogenide glasses are shown to have great promise for use as diffracting elements in the red to far infrared (up to 15 μm). In principle, they are simple to fabricate - phase gratings being produced by mask exposure or holographic techniques. The performance of bulk, rectangular phase gratings is investigated using a coupled wave model and a detailed analysis performed in the thin, multiwave and volume diffraction regimes. High efficiencies (> 97%) are found to be achievable in the multiwave regime. Based on available material data for silver doped arsenic sulphide glasses, the optimum parameters for operation at 632.8 nm, 4 μm and 10.6 μm are calculated. The maximum efficiencies likely to be achieved and angular responses are evaluated.